SUPPORTING INFORMATION

A Combinatorial NMR and EPR Approach for Evaluating the Structural Ensemble of Partially Folded Proteins

Jampani Nageswara Rao, Christine C. Jao, Balachandra G. Hegde, Ralf Langen and Tobias S. Ulmer

Department of Biochemistry & Molecular Biology, Zilkha Neurogenetic Institute, Keck School of Medicine, University of Southern California, 1501 San Pablo Street, Los Angeles, California 90033

TABLE OF CONTENTS

Supplementary Table 1. ϕ, ψ dihedral angles of SLAS-bound αS from molecular fragment replacement

Residue	Name	PHI	PSI	ΔPHI	ΔPSI
2	D	-74.0	-26.2	10.6	10.5
3	V	-71.9	-31.0	8.8	3.6
4	F	-74.0	-39.7	8.1	4.5
5	M	-65.1	-38.9	4.4	4.2
6	K	-66.2	-41.8	5.6	5.5
7	G	-67.5	-38.6	6.7	4.4
8	L	-64.5	-43.8	5.4	6.0
9	S	-64.3	-38.3	5.4	6.9
10	K	-64.5	-44.8	6.5	4.4
11	A	-64.1	-41.1	3.6	2.9
12	K	-61.1	-44.2	2.3	3.6
13	E	-64.3	-38.9	3.5	4.0
14	G	-66.3	-39.8	3.1	3.5
15	V	-64.8	-41.4	3.5	2.4
16	V	-63.8	-45.6	2.7	2.9
17	A	-62.5	-40.0	3.9	4.6
18	A	-67.7	-39.7	4.0	2.7
19	A	-63.3	-44.2	2.4	4.8
20	E	-66.2	-38.7	5.0	5.9
21	K	-68.9	-38.2	5.2	4.9
22	T	-67.2	-37.7	4.8	3.7
23	K	-66.7	-33.9	5.7	12.5
24	Q	-68.0	-36.0	13.8	11.1
25	G	-66.4	-32.5	5.6	6.2
26	V	-70.9	-37.1	6.6	8.4
27	A	-65.8	-39.2	5.6	11.1
28	E	-70.4	-31.7	7.8	11.9
29	A	-67.9	-29.3	6.2	8.0
30	A	-70.1	-22.2	8.7	11.7
31	G	-79.5	-8.6	17.9	15.2
32	K	-80.1	-14.0	11.3	15.0
42	S	-60.3	-29.7	8.0	11.2
43	K	-69.2	-29.9	8.2	12.8
44	T	-73.3	-29.6	8.2	7.8
45	K	-61.5	-44.0	7.2	7.0
46	E	-69.5	-36.4	4.0	4.2
47	G	-65.9	-41.3	3.9	6.2
48	V	-65.9	-43.9	5.3	5.9
49	V	-66.2	-42.4	4.3	3.9
50	H	-64.8	-36.4	4.1	3.3
51	G	-63.7	-43.7	3.3	5.5
52	V	-64.8	-42.0	4.8	5.0
53	A	-63.0	-38.3	4.9	5.8
54	T	-68.9	-37.4	8.3	9.8
55	V	-61.5	-44.6	11.8	10.5
56	A	-58.8	-42.9	8.6	11.1

57	E	-62.5	-36.0	7.1	4.6
58	K	-73.9	-44.0	4.5	7.9
59	T	-63.4	-36.3	6.8	6.5
60	K	-63.6	-40.7	5.8	7.2
61	E	-67.6	-36.6	5.1	5.5
62	Q	-67.4	-38.5	3.9	8.0
63	V	-62.3	-41.4	5.4	6.5
64	T	-66.2	-35.9	5.4	5.3
65	N	-70.8	-38.0	11.0	9.5
66	V	-74.6	-33.5	9.5	7.6
67	G	-60.2	-43.3	6.9	9.7
68	G	-65.5	-40.0	8.6	6.6
69	A	-65.9	-41.3	6.8	5.6
70	V	-64.8	-42.0	4.6	4.7
71	V	-64.2	-43.9	4.3	4.8
72	T	-61.5	-43.1	4.8	4.7
73	G	-64.3	-42.9	3.8	3.0
74	V	-65.9	-37.4	3.2	4.6
75	T	-66.7	-39.5	4.0	4.7
76	A	-65.7	-38.4	4.6	4.2
77	V	-69.2	-41.1	3.3	3.5
78	A	-61.3	-40.7	3.8	5.1
79	Q	-66.9	-42.2	4.9	5.4
80	K	-65.4	-33.7	4.9	2.9
81	T	-67.6	-37.6	3.2	5.9
82	V	-66.5	-39.3	5.5	5.7
83	E	-69.0	-37.4	9.5	8.8
84	G	-72.2	-29.5	11.5	6.2
85	A	-55.4	-33.1	10.1	15.2
86	G	-60.2	-40.5	8.7	5.5
87	S	-69.6	-33.4	4.9	5.3
88	I	-66.8	-38.7	3.7	5.1
89	A	-63.3	-43.2	3.8	3.7
90	A	-64.7	-39.9	5.3	5.1
91	A	-68.2	-29.2	7.5	9.9
92	T	-79.6	-14.8	14.5	20.7

Supplementary Table 2. Possible subpopulation combinations of observed spin label interelectron distance distribution maxima[a]

Subset	11-26	11-41	11-70	11-72	11-81	11-83	22-52	26-41	26-56	37-67	41-56	41-67	41-70	44-67	48-67	56-70	56-85	63-81
1	23.0	31.0	22.5	28.5	20.0	25.5	29.0	23.5	20.5	23.5	24.5	25.0	29.0	23.0	21.5	19.5	37.0	28.0
2	23.0	31.0	22.5	28.5	20.0	25.5	29.0	23.5	20.5	23.5	24.5	25.0	29.0	23.0	27.5	19.5	37.0	28.0
3	23.0	31.0	22.5	28.5	20.0	25.5	29.0	23.5	20.5	26.5	24.5	25.0	29.0	23.0	21.5	19.5	37.0	28.0
4	23.0	31.0	22.5	28.5	20.0	25.5	29.0	23.5	20.5	26.5	24.5	25.0	29.0	23.0	27.5	19.5	37.0	28.0
5	23.0	31.0	22.5	28.5	20.0	25.5	29.0	23.5	20.5	37.5	24.5	25.0	29.0	23.0	21.5	19.5	37.0	28.0
6	23.0	31.0	22.5	28.5	20.0	25.5	29.0	23.5	20.5	37.5	24.5	25.0	29.0	23.0	27.5	19.5	37.0	28.0
7	23.0	31.0	22.5	28.5	20.0	25.5	29.0	23.5	29.0	23.5	24.5	25.0	29.0	23.0	21.5	19.5	37.0	28.0
8	23.0	31.0	22.5	28.5	20.0	25.5	29.0	23.5	29.0	23.5	24.5	25.0	29.0	23.0	27.5	19.5	37.0	28.0
9	23.0	31.0	22.5	28.5	20.0	25.5	29.0	23.5	29.0	26.5	24.5	25.0	29.0	23.0	21.5	19.5	37.0	28.0
10	23.0	31.0	22.5	28.5	20.0	25.5	29.0	23.5	29.0	26.5	24.5	25.0	29.0	23.0	27.5	19.5	37.0	28.0
11	23.0	31.0	22.5	28.5	20.0	25.5	29.0	23.5	29.0	37.5	24.5	25.0	29.0	23.0	21.5	19.5	37.0	28.0
12	23.0	31.0	22.5	28.5	20.0	25.5	29.0	23.5	29.0	37.5	24.5	25.0	29.0	23.0	27.5	19.5	37.0	28.0
13	23.0	31.0	22.5	28.5	25.5	25.5	29.0	23.5	20.5	23.5	24.5	25.0	29.0	23.0	21.5	19.5	37.0	28.0
14	23.0	31.0	22.5	28.5	25.5	25.5	29.0	23.5	20.5	23.5	24.5	25.0	29.0	23.0	27.5	19.5	37.0	28.0
15	23.0	31.0	22.5	28.5	25.5	25.5	29.0	23.5	20.5	26.5	24.5	25.0	29.0	23.0	21.5	19.5	37.0	28.0
16	23.0	31.0	22.5	28.5	25.5	25.5	29.0	23.5	20.5	26.5	24.5	25.0	29.0	23.0	27.5	19.5	37.0	28.0
17	23.0	31.0	22.5	28.5	25.5	25.5	29.0	23.5	20.5	37.5	24.5	25.0	29.0	23.0	21.5	19.5	37.0	28.0
18	23.0	31.0	22.5	28.5	25.5	25.5	29.0	23.5	20.5	37.5	24.5	25.0	29.0	23.0	27.5	19.5	37.0	28.0
19	23.0	31.0	22.5	28.5	25.5	25.5	29.0	23.5	29.0	23.5	24.5	25.0	29.0	23.0	21.5	19.5	37.0	28.0
20	23.0	31.0	22.5	28.5	25.5	25.5	29.0	23.5	29.0	23.5	24.5	25.0	29.0	23.0	27.5	19.5	37.0	28.0
21	23.0	31.0	22.5	28.5	25.5	25.5	29.0	23.5	29.0	26.5	24.5	25.0	29.0	23.0	21.5	19.5	37.0	28.0
22	23.0	31.0	22.5	28.5	25.5	25.5	29.0	23.5	29.0	26.5	24.5	25.0	29.0	23.0	27.5	19.5	37.0	28.0
23	23.0	31.0	22.5	28.5	25.5	25.5	29.0	23.5	29.0	37.5	24.5	25.0	29.0	23.0	21.5	19.5	37.0	28.0
24	23.0	31.0	22.5	28.5	25.5	25.5	29.0	23.5	29.0	37.5	24.5	25.0	29.0	23.0	27.5	19.5	37.0	28.0
25	23.0	31.0	27.5	28.5	20.0	25.5	29.0	23.5	20.5	23.5	24.5	25.0	29.0	23.0	21.5	19.5	37.0	28.0
26	23.0	31.0	27.5	28.5	20.0	25.5	29.0	23.5	20.5	23.5	24.5	25.0	29.0	23.0	27.5	19.5	37.0	28.0
27	23.0	31.0	27.5	28.5	20.0	25.5	29.0	23.5	20.5	26.5	24.5	25.0	29.0	23.0	21.5	19.5	37.0	28.0
28	23.0	31.0	27.5	28.5	20.0	25.5	29.0	23.5	20.5	26.5	24.5	25.0	29.0	23.0	27.5	19.5	37.0	28.0
29	23.0	31.0	27.5	28.5	20.0	25.5	29.0	23.5	20.5	37.5	24.5	25.0	29.0	23.0	21.5	19.5	37.0	28.0
30	23.0	31.0	27.5	28.5	20.0	25.5	29.0	23.5	20.5	37.5	24.5	25.0	29.0	23.0	27.5	19.5	37.0	28.0
31	23.0	31.0	27.5	28.5	20.0	25.5	29.0	23.5	29.0	23.5	24.5	25.0	29.0	23.0	21.5	19.5	37.0	28.0
32	23.0	31.0	27.5	28.5	20.0	25.5	29.0	23.5	29.0	23.5	24.5	25.0	29.0	23.0	27.5	19.5	37.0	28.0
33	23.0	31.0	27.5	28.5	20.0	25.5	29.0	23.5	29.0	26.5	24.5	25.0	29.0	23.0	21.5	19.5	37.0	28.0
34	23.0	31.0	27.5	28.5	20.0	25.5	29.0	23.5	29.0	26.5	24.5	25.0	29.0	23.0	27.5	19.5	37.0	28.0
35	23.0	31.0	27.5	28.5	20.0	25.5	29.0	23.5	29.0	37.5	24.5	25.0	29.0	23.0	21.5	19.5	37.0	28.0
36	23.0	31.0	27.5	28.5	20.0	25.5	29.0	23.5	29.0	37.5	24.5	25.0	29.0	23.0	27.5	19.5	37.0	28.0
37	23.0	31.0	27.5	28.5	25.5	25.5	29.0	23.5	20.5	23.5	24.5	25.0	29.0	23.0	21.5	19.5	37.0	28.0
38	23.0	31.0	27.5	28.5	25.5	25.5	29.0	23.5	20.5	23.5	24.5	25.0	29.0	23.0	27.5	19.5	37.0	28.0
39	23.0	31.0	27.5	28.5	25.5	25.5	29.0	23.5	20.5	26.5	24.5	25.0	29.0	23.0	21.5	19.5	37.0	28.0
40	23.0	31.0	27.5	28.5	25.5	25.5	29.0	23.5	20.5	26.5	24.5	25.0	29.0	23.0	27.5	19.5	37.0	28.0
41	23.0	31.0	27.5	28.5	25.5	25.5	29.0	23.5	20.5	37.5	24.5	25.0	29.0	23.0	21.5	19.5	37.0	28.0
42	23.0	31.0	27.5	28.5	25.5	25.5	29.0	23.5	20.5	37.5	24.5	25.0	29.0	23.0	27.5	19.5	37.0	28.0
43	23.0	31.0	27.5	28.5	25.5	25.5	29.0	23.5	29.0	23.5	24.5	25.0	29.0	23.0	21.5	19.5	37.0	28.0
44	23.0	31.0	27.5	28.5	25.5	25.5	29.0	23.5	29.0	23.5	24.5	25.0	29.0	23.0	27.5	19.5	37.0	28.0
45	23.0	31.0	27.5	28.5	25.5	25.5	29.0	23.5	29.0	26.5	24.5	25.0	29.0	23.0	21.5	19.5	37.0	28.0
46	23.0	31.0	27.5	28.5	25.5	25.5	29.0	23.5	29.0	26.5	24.5	25.0	29.0	23.0	27.5	19.5	37.0	28.0

47	23.0	31.0	27.5	28.5	25.5	25.5	29.0	23.5	29.0	37.5	24.5	25.0	29.0	23.0	21.5	19.5	37.0	28.0
48	23.0	31.0	27.5	28.5	25.5	25.5	29.0	23.5	29.0	37.5	24.5	25.0	29.0	23.0	27.5	19.5	37.0	28.0
49	23.0	40.5	22.5	28.5	20.0	25.5	29.0	23.5	20.5	23.5	24.5	25.0	29.0	23.0	21.5	19.5	37.0	28.0
50	23.0	40.5	22.5	28.5	20.0	25.5	29.0	23.5	20.5	23.5	24.5	25.0	29.0	23.0	27.5	19.5	37.0	28.0
51	23.0	40.5	22.5	28.5	20.0	25.5	29.0	23.5	20.5	26.5	24.5	25.0	29.0	23.0	21.5	19.5	37.0	28.0
52	23.0	40.5	22.5	28.5	20.0	25.5	29.0	23.5	20.5	26.5	24.5	25.0	29.0	23.0	27.5	19.5	37.0	28.0
53	23.0	40.5	22.5	28.5	20.0	25.5	29.0	23.5	20.5	37.5	24.5	25.0	29.0	23.0	21.5	19.5	37.0	28.0
54	23.0	40.5	22.5	28.5	20.0	25.5	29.0	23.5	20.5	37.5	24.5	25.0	29.0	23.0	27.5	19.5	37.0	28.0
55	23.0	40.5	22.5	28.5	20.0	25.5	29.0	23.5	29.0	23.5	24.5	25.0	29.0	23.0	21.5	19.5	37.0	28.0
56	23.0	40.5	22.5	28.5	20.0	25.5	29.0	23.5	29.0	23.5	24.5	25.0	29.0	23.0	27.5	19.5	37.0	28.0
57	23.0	40.5	22.5	28.5	20.0	25.5	29.0	23.5	29.0	26.5	24.5	25.0	29.0	23.0	21.5	19.5	37.0	28.0
58	23.0	40.5	22.5	28.5	20.0	25.5	29.0	23.5	29.0	26.5	24.5	25.0	29.0	23.0	27.5	19.5	37.0	28.0
59	23.0	40.5	22.5	28.5	20.0	25.5	29.0	23.5	29.0	37.5	24.5	25.0	29.0	23.0	21.5	19.5	37.0	28.0
60	23.0	40.5	22.5	28.5	20.0	25.5	29.0	23.5	29.0	37.5	24.5	25.0	29.0	23.0	27.5	19.5	37.0	28.0
61	23.0	40.5	22.5	28.5	25.5	25.5	29.0	23.5	20.5	23.5	24.5	25.0	29.0	23.0	21.5	19.5	37.0	28.0
62	23.0	40.5	22.5	28.5	25.5	25.5	29.0	23.5	20.5	23.5	24.5	25.0	29.0	23.0	27.5	19.5	37.0	28.0
63	23.0	40.5	22.5	28.5	25.5	25.5	29.0	23.5	20.5	26.5	24.5	25.0	29.0	23.0	21.5	19.5	37.0	28.0
64	23.0	40.5	22.5	28.5	25.5	25.5	29.0	23.5	20.5	26.5	24.5	25.0	29.0	23.0	27.5	19.5	37.0	28.0
65	23.0	40.5	22.5	28.5	25.5	25.5	29.0	23.5	20.5	37.5	24.5	25.0	29.0	23.0	21.5	19.5	37.0	28.0
66	23.0	40.5	22.5	28.5	25.5	25.5	29.0	23.5	20.5	37.5	24.5	25.0	29.0	23.0	27.5	19.5	37.0	28.0
67	23.0	40.5	22.5	28.5	25.5	25.5	29.0	23.5	29.0	23.5	24.5	25.0	29.0	23.0	21.5	19.5	37.0	28.0
68	23.0	40.5	22.5	28.5	25.5	25.5	29.0	23.5	29.0	23.5	24.5	25.0	29.0	23.0	27.5	19.5	37.0	28.0
69	23.0	40.5	22.5	28.5	25.5	25.5	29.0	23.5	29.0	26.5	24.5	25.0	29.0	23.0	21.5	19.5	37.0	28.0
70	23.0	40.5	22.5	28.5	25.5	25.5	29.0	23.5	29.0	26.5	24.5	25.0	29.0	23.0	27.5	19.5	37.0	28.0
71	23.0	40.5	22.5	28.5	25.5	25.5	29.0	23.5	29.0	37.5	24.5	25.0	29.0	23.0	21.5	19.5	37.0	28.0
72	23.0	40.5	22.5	28.5	25.5	25.5	29.0	23.5	29.0	37.5	24.5	25.0	29.0	23.0	27.5	19.5	37.0	28.0
73	23.0	40.5	27.5	28.5	20.0	25.5	29.0	23.5	20.5	23.5	24.5	25.0	29.0	23.0	21.5	19.5	37.0	28.0
74	23.0	40.5	27.5	28.5	20.0	25.5	29.0	23.5	20.5	23.5	24.5	25.0	29.0	23.0	27.5	19.5	37.0	28.0
75	23.0	40.5	27.5	28.5	20.0	25.5	29.0	23.5	20.5	26.5	24.5	25.0	29.0	23.0	21.5	19.5	37.0	28.0
76	23.0	40.5	27.5	28.5	20.0	25.5	29.0	23.5	20.5	26.5	24.5	25.0	29.0	23.0	27.5	19.5	37.0	28.0
77	23.0	40.5	27.5	28.5	20.0	25.5	29.0	23.5	20.5	37.5	24.5	25.0	29.0	23.0	21.5	19.5	37.0	28.0
78	23.0	40.5	27.5	28.5	20.0	25.5	29.0	23.5	20.5	37.5	24.5	25.0	29.0	23.0	27.5	19.5	37.0	28.0
79	23.0	40.5	27.5	28.5	20.0	25.5	29.0	23.5	29.0	23.5	24.5	25.0	29.0	23.0	21.5	19.5	37.0	28.0
80	23.0	40.5	27.5	28.5	20.0	25.5	29.0	23.5	29.0	23.5	24.5	25.0	29.0	23.0	27.5	19.5	37.0	28.0
81	23.0	40.5	27.5	28.5	20.0	25.5	29.0	23.5	29.0	26.5	24.5	25.0	29.0	23.0	21.5	19.5	37.0	28.0
82	23.0	40.5	27.5	28.5	20.0	25.5	29.0	23.5	29.0	26.5	24.5	25.0	29.0	23.0	27.5	19.5	37.0	28.0
83	23.0	40.5	27.5	28.5	20.0	25.5	29.0	23.5	29.0	37.5	24.5	25.0	29.0	23.0	21.5	19.5	37.0	28.0
84	23.0	40.5	27.5	28.5	20.0	25.5	29.0	23.5	29.0	37.5	24.5	25.0	29.0	23.0	27.5	19.5	37.0	28.0
85	23.0	40.5	27.5	28.5	25.5	25.5	29.0	23.5	20.5	23.5	24.5	25.0	29.0	23.0	21.5	19.5	37.0	28.0
86	23.0	40.5	27.5	28.5	25.5	25.5	29.0	23.5	20.5	23.5	24.5	25.0	29.0	23.0	27.5	19.5	37.0	28.0
87	23.0	40.5	27.5	28.5	25.5	25.5	29.0	23.5	20.5	26.5	24.5	25.0	29.0	23.0	21.5	19.5	37.0	28.0
88	23.0	40.5	27.5	28.5	25.5	25.5	29.0	23.5	20.5	26.5	24.5	25.0	29.0	23.0	27.5	19.5	37.0	28.0
89	23.0	40.5	27.5	28.5	25.5	25.5	29.0	23.5	20.5	37.5	24.5	25.0	29.0	23.0	21.5	19.5	37.0	28.0
90	23.0	40.5	27.5	28.5	25.5	25.5	29.0	23.5	20.5	37.5	24.5	25.0	29.0	23.0	27.5	19.5	37.0	28.0
91	23.0	40.5	27.5	28.5	25.5	25.5	29.0	23.5	29.0	23.5	24.5	25.0	29.0	23.0	21.5	19.5	37.0	28.0
92	23.0	40.5	27.5	28.5	25.5	25.5	29.0	23.5	29.0	23.5	24.5	25.0	29.0	23.0	27.5	19.5	37.0	28.0
93	23.0	40.5	27.5	28.5	25.5	25.5	29.0	23.5	29.0	26.5	24.5	25.0	29.0	23.0	21.5	19.5	37.0	28.0
94	23.0	40.5	27.5	28.5	25.5	25.5	29.0	23.5	29.0	26.5	24.5	25.0	29.0	23.0	27.5	19.5	37.0	28.0
95	23.0	40.5	27.5	28.5	25.5	25.5	29.0	23.5	29.0	37.5	24.5	25.0	29.0	23.0	21.5	19.5	37.0	28.0
96	23.0	40.5	27.5	28.5	25.5	25.5	29.0	23.5	29.0	37.5	24.5	25.0	29.0	23.0	27.5	19.5	37.0	28.0

[a]EPR-derived interelectron distances are given in Ångstrøm

Supplementary Table 3. Comparison of expected and actual R1 χ_{1-3} distributions in $R^2(0.990)$ ensemble[a]

Residue	Number of structures with χ_{1-3} combination #1[b]	Number of structures with χ_{1-3} combination #2	Number of structures with χ_{1-3} combination #3	Number of structures with χ_{1-3} combination #4	Number of structures with χ_{1-3} combination #5
11	4503	4419	4438	2300	2172
22	4454	4470	4437	2257	2224
26	4426	4478	4449	2259	2234
37	4429	4472	4505	2229	2203
41	4418	4578	4417	2235	2187
44	4395	4401	4616	2210	2224
48	4425	4546	4412	2267	2195
52	4506	4513	4361	2267	2181
56	4482	4433	4515	2237	2181
63	4439	4581	4439	2248	2140
67	4448	4558	4422	2188	2229
70	4406	4611	4394	2220	2215
72	4541	4454	4488	2177	2178
81	4357	4541	4386	2286	2279
83	4461	4501	4450	2181	2247
85	4519	4368	4487	2230	2242
expected	4466	4466	4466	2233	2233

Residue	Percentage of structures with expected χ_{1-3} combination #1[a]	Percentage of structures with expected χ_{1-3} combination #2	Percentage of structures with expected χ_{1-3} combination #3	Percentage of structures with expected χ_{1-3} combination #4	Percentage of structures with expected χ_{1-3} combination #5
11	100.8	98.9	99.4	103	97.3
22	99.7	100.1	99.3	101.1	99.6
26	99.1	100.3	99.6	101.1	100
37	99.2	100.1	100.9	99.8	98.6
41	98.9	102.5	98.9	100.1	97.9
44	98.4	98.5	103.3	99	99.6
48	99.1	101.8	98.8	101.5	98.3
52	100.9	101	97.6	101.5	97.7
56	100.3	99.2	101.1	100.2	97.7
63	99.4	102.6	99.4	100.7	95.8
67	99.6	102	99	98	99.8
70	98.6	103.2	98.4	99.4	99.2
72	101.7	99.7	100.5	97.5	97.5
81	97.5	101.7	98.2	102.4	102
83	99.9	100.8	99.6	97.7	100.6
85	101.2	97.8	100.5	99.8	100.4

a, Spin label rotamers were assigned in the initial ensemble consisting of 60,000 structures. The $R^2(0.990)$ ensemble consists of 17,867 structures.

b, #1-5 denote χ_{1-3} combinations -60°, -60°, +90°; -60°, -60°, -90°; 180°, -60°, -90°; 180°, +60°, +90°; and 180°, +60°, -90°, respectively, of a MTSL spin-labeled residue.

Supplementary Table 4. Ratio of helix configurations in SLAS-bound αS subpopulations[a]

Subpopulation	N′C′/opposite[b] [%]	N′C′/same [%]	C′N′/opposite [%]	C′N′/same [%]
9	42.2	15.8	5.1	36.9
11	43.1	16.4	6.5	34.0
21	35.4	20.0	9.9	34.7
23	35.3	22.2	10.8	31.8
33	38.4	14.7	6.9	39.9
35	40.0	16.7	8.4	34.9
45	31.6	12.6	6.9	36.6
47	34.6	20.4	15.4	29.6
57	33.3	17.6	5.4	43.6
59	33.3	20.2	7.0	39.6
69	28.8	21.8	8.8	40.6
71	29.3	23.5	11.5	35.7
81	31.5	16.5	7.4	44.5
82	31.9	18.8	8.6	40.6
91	24.9	20.2	12.0	42.9
93	25.1	20.4	12.7	41.8
95	27.0	23.5	14.9	34.6

a, A total of 5,000 structures were calculated for each subpopulation.
b, Helix configuration selection criteria are described in Fig. 6.

Supplementary Table 5. Comparison of backbone r.m.s. deviations between subpopulation C′N′/same average representatives.

Subpopulation[a,b,c]	9	11	21	23	33	35	45	47	57	59	69	71	81	83	91	95	93	r.m.s.d. to mean coordinates[d]	number of structures[e]
9	0.0	1.8	1.9	2.7	2.2	1.6	2.9	2.3	2.5	1.5	1.0	1.9	2.7	1.8	2.5	1.0	2.0	4.5	1791
11		0.0	1.2	2.1	1.8	1.1	2.7	1.6	3.0	1.5	1.6	1.4	3.2	2.4	2.9	2.1	2.9	4.1	1650
21			0.0	2.3	1.9	1.1	2.6	1.8	3.0	2.0	1.6	1.9	3.3	2.6	3.1	2.1	2.9	4.6	1680
23				0.0	3.1	2.0	3.6	1.8	4.3	2.4	2.8	2.4	4.9	3.8	4.6	3.3	4.1	4.4	1534
33					0.0	1.9	2.8	2.1	2.3	1.8	1.8	1.5	2.6	1.5	2.1	2.0	1.9	4.8	1929
35						0.0	2.4	1.3	2.8	1.4	1.4	1.3	3.2	2.3	3.0	1.9	2.7	4.5	1686
45							0.0	2.8	3.2	2.8	2.8	3.1	3.3	3.0	3.4	2.9	3.5	5.0	1762
47								0.0	3.6	2.0	1.9	1.7	3.9	2.8	3.5	2.5	3.2	4.6	1433
57									0.0	2.2	2.6	2.6	1.7	1.7	1.9	2.1	1.8	4.1	2122
59										0.0	1.7	1.1	2.9	1.9	2.6	1.6	2.2	3.9	1926
69											0.0	1.6	2.7	1.7	2.3	1.0	1.9	4.4	1966
71												0.0	3.1	2.0	2.6	1.8	2.3	4.1	1728
81													0.0	1.7	1.3	2.3	2.0	4.3	2171
83														0.0	1.3	1.4	1.0	4.1	1976
91															0.0	1.9	1.6	4.6	2076
95																0.0	1.5	4.3	1682
93																	0.0	4.6	1974

a, Subpopulations were calculated with a distance interval/grace margin of ±2.5/0.5 Å, and are represented by the closest structure to the backbone N, C^{α}, C′ mean coordinates of residues 2-32 (helix-N′) and 42-92 (helix-C′) of structures in C′N′/same helix order (c.f. Fig. 7).

b, For subsets populating the lowest 37R1-67R1 distance maximum (Supplementary Fig. 5), only subset combination 91 is represented due to the high similarity to subsets with a 37R1-67R1 center maximum.

c, The subset average representatives have been deposited in the Protein Data Bank (accession number 2kkw) in the depicted order, i.e., subpopulation 9 corresponds to model 1. The average representatives in N′C′/same orientation were also included in the same order, starting with model 18. The two basis structures (see main text) are represented by model 1 (subpopulation 9 in C′N′/same order) and model 34 (subpopulation 93 in N′C′/same order).

d, Denotes the root-mean-square-deviation of all C′N′/same subpopulation structures to the mean backbone N, C^{α}, C′ coordinates of residues 2-32 (helix-N′) and 42-92 (helix-C′).

e, Number of structures in subset in C′N′/same orientation out of a total of 5,000 calculated structures.

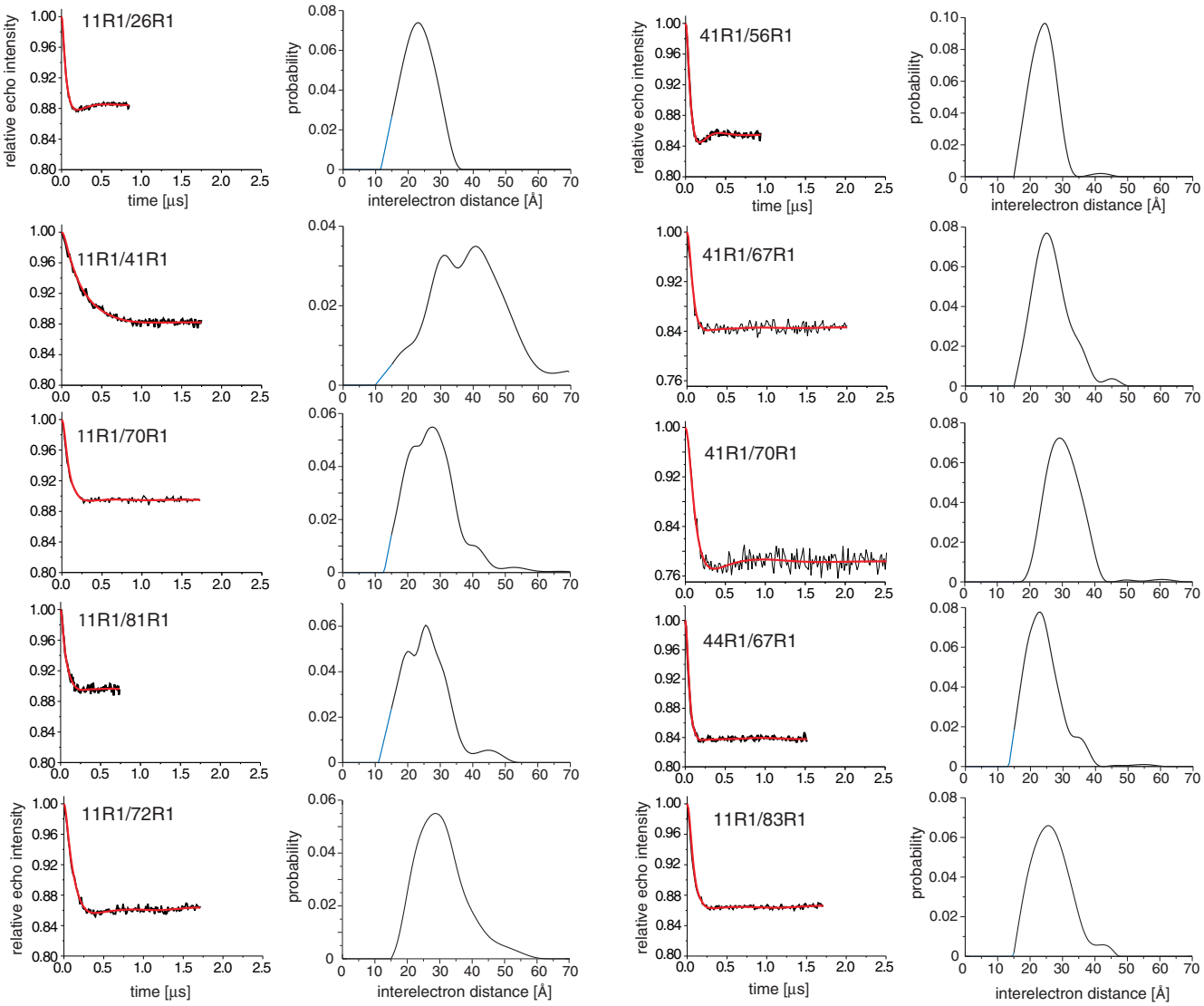

Supplementary Figure 1. Spin label interelectron distances from 4-pulse DEER experiments. The first and third columns depict the dipolar evolution for each of the indicated spin label pair. The *black* traces denote background-corrected experimental data. The *red* curves depict fits using L-curve Tikhonov regularizations and the second and fourth columns show the resulting interelectron distance distributions in *black*. Below 15 Å distances cannot readily be detected by 4-pulse DEER experiments because of their strongly reduced modulation depth.[1] To reach zero probability, distributions were extrapolated below 15 Å (*blue* curve). This extrapolation, which is desirable for a few distance pairs, does not affect the conclusions drawn in the present study. The distance distributions were integrated and assigned overall probabilities of 1. Minor distribution peaks at low probabilities arise from imperfect background corrections and are unlikely to be of significance. To optimize signal-to-noise ratios, short acquisition times were used for shorter distances and long acquisition times were used for longer distances for which dipolar evolutions are of lower frequency. For shorter distance scans, the baseline correction was verified by scans of longer time base. Because of significantly better signal-to-noise ratios, however, shorter scans were used to carry out Tikhonov regularization. The increased uncertainty arising from shortened time scans was compensated by enhanced signal-to-noise ratios.

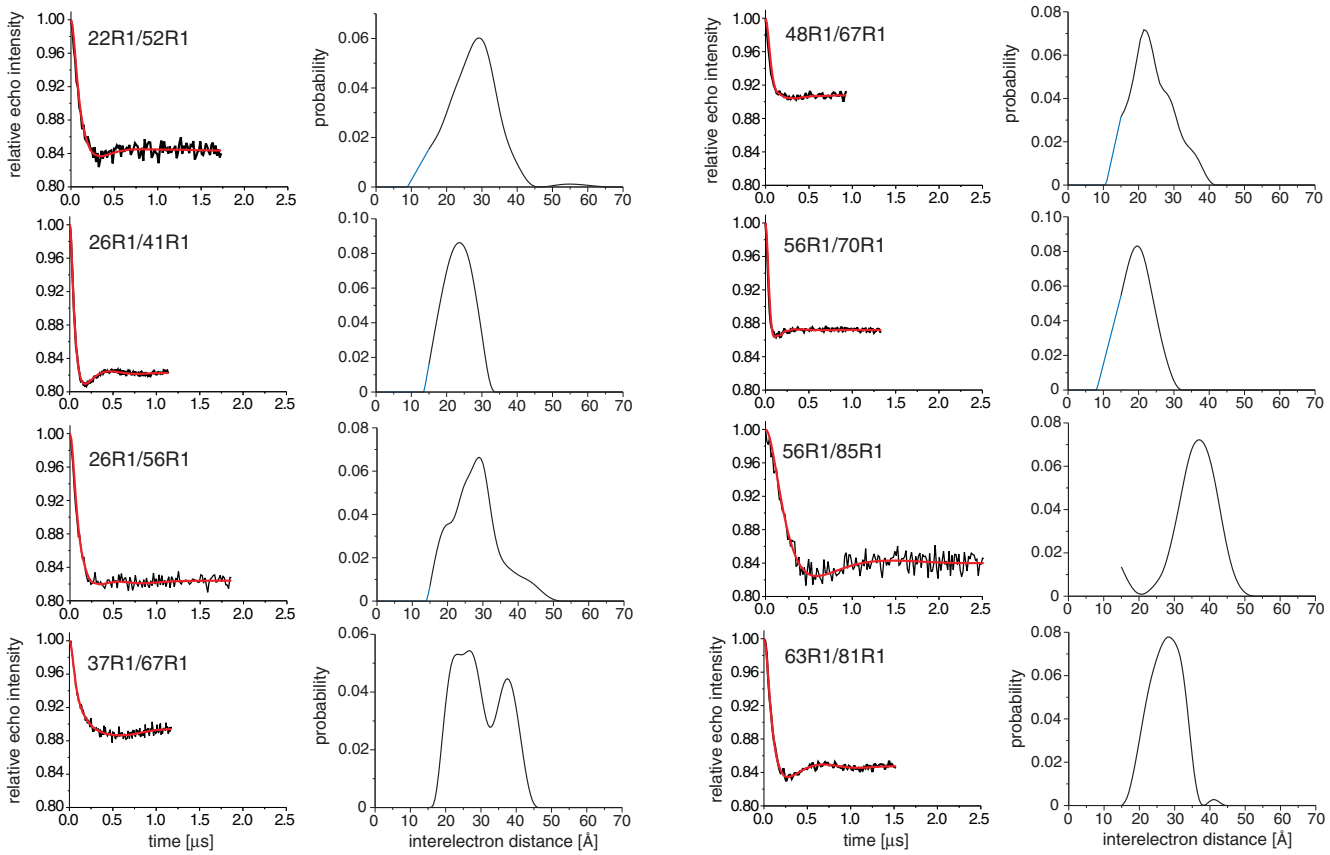

Supplementary Figure 1. continued

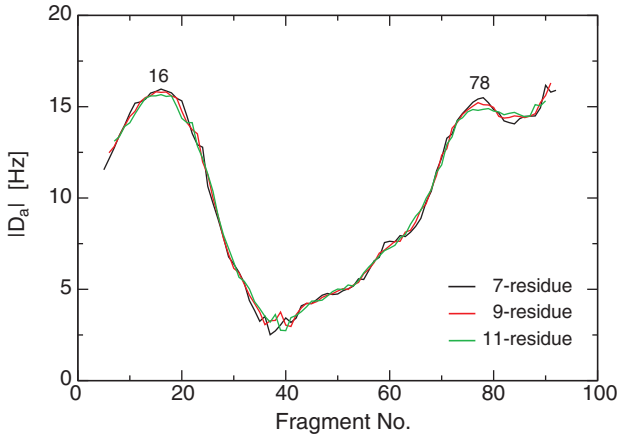

Supplementary Figure 2 Variation of alignment tensor magnitude, D_a, with fragment length. The fragment number is the center residue number of each fragment. No significant changes in D_a values were obtained for fragment lengths of 7, 9 and 11 residues. Residual dipolar couplings (RDC) measured in 5.2% polyacrylamide gels were used to calculate alignment tensor parameter. The two other couplings datasets exhibit normalized scalar product to this dataset not lower than 0.98. For residues 10-18 and 74-81, which exhibit comparable D_a values, RDC were described by a common alignment tensor.

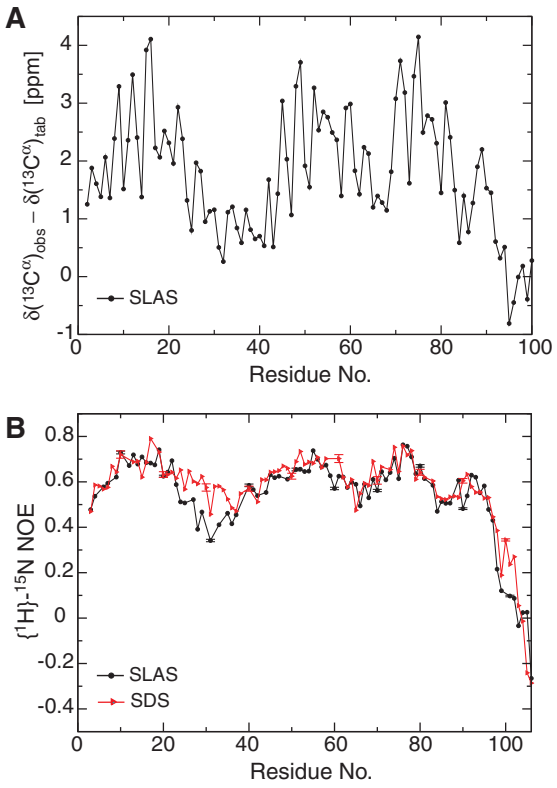

Supplementary Figure 3. Structural and dynamic NMR parameter of SLAS-bound αS. (**A**) Backbone secondary structure propensities as reflected by secondary $^{13}C^{\alpha}$ chemical shifts. For $^{2}H/^{13}C/^{15}N$-labeled αS, random coil conformations are obtained at approximately −0.5 ppm, whereas positive and negative shifts relative to this value denote helical and extended backbone propensities, respectively.[2,3] (**B**) Comparison of SDS- and SLAS-bound αS backbone order (pico- to nanosecond timescale dynamics) as reported by $\{^{1}H\}$-^{15}N NOE values at a ^{15}N frequency of 70.9 MHz. Larger values denote smaller amplitude H-N amide bond vector dynamics.[4]

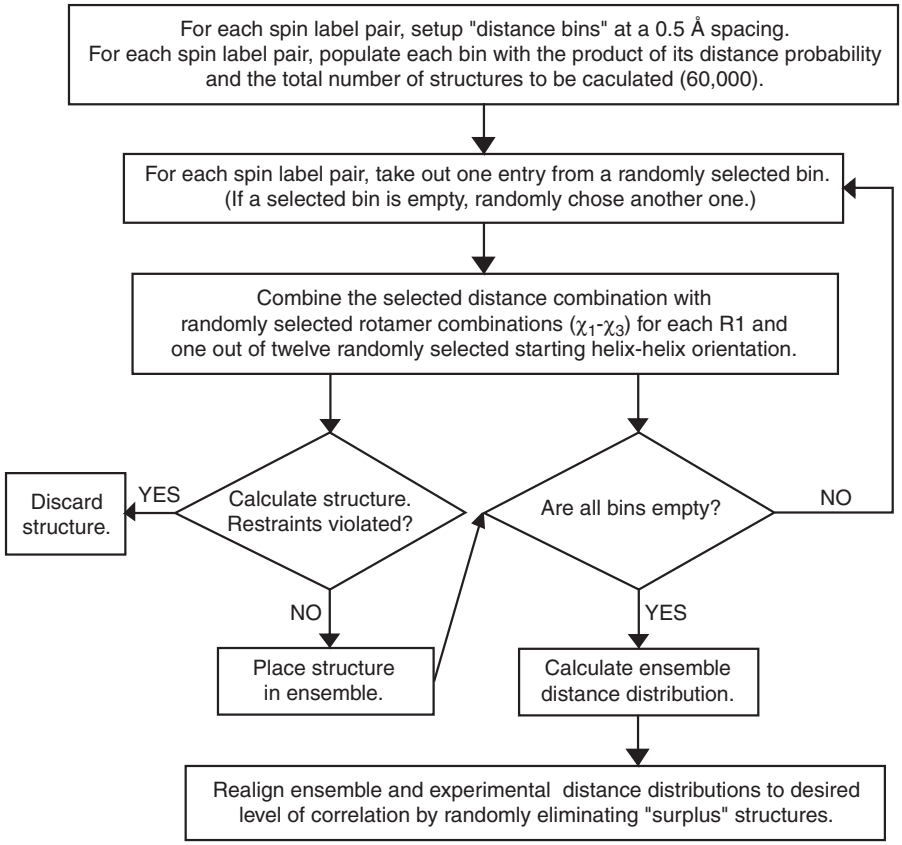

Supplementary Figure 4. Flowchart of ensemble structure calculation scheme. To create a distance distribution reconstruction template utilizing only the $P_c > P_i$ condition, the step of calculating structures and testing restraint violations as well as all subsequent steps can be eliminated.

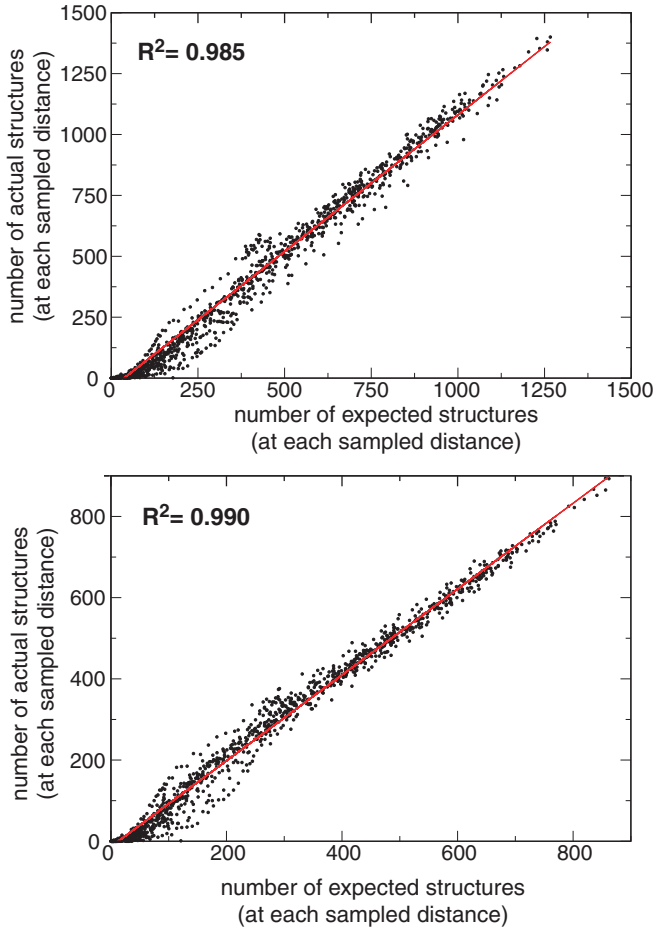

Supplementary Figure 5. Correlation between the number of expected and obtained ensemble structures at each sampled interelectron distance. At each of the 141 sampled distances in the 0-70 Å range (0.5 Å resolution), the number of obtained ensemble structures was correlated to the number of expected structures. The depicted correlations encompass all 18 measured interelectron distance distributions (Supplementary Fig. 1). The same data is shown "uncluttered" in Supplementary Fig. 6.

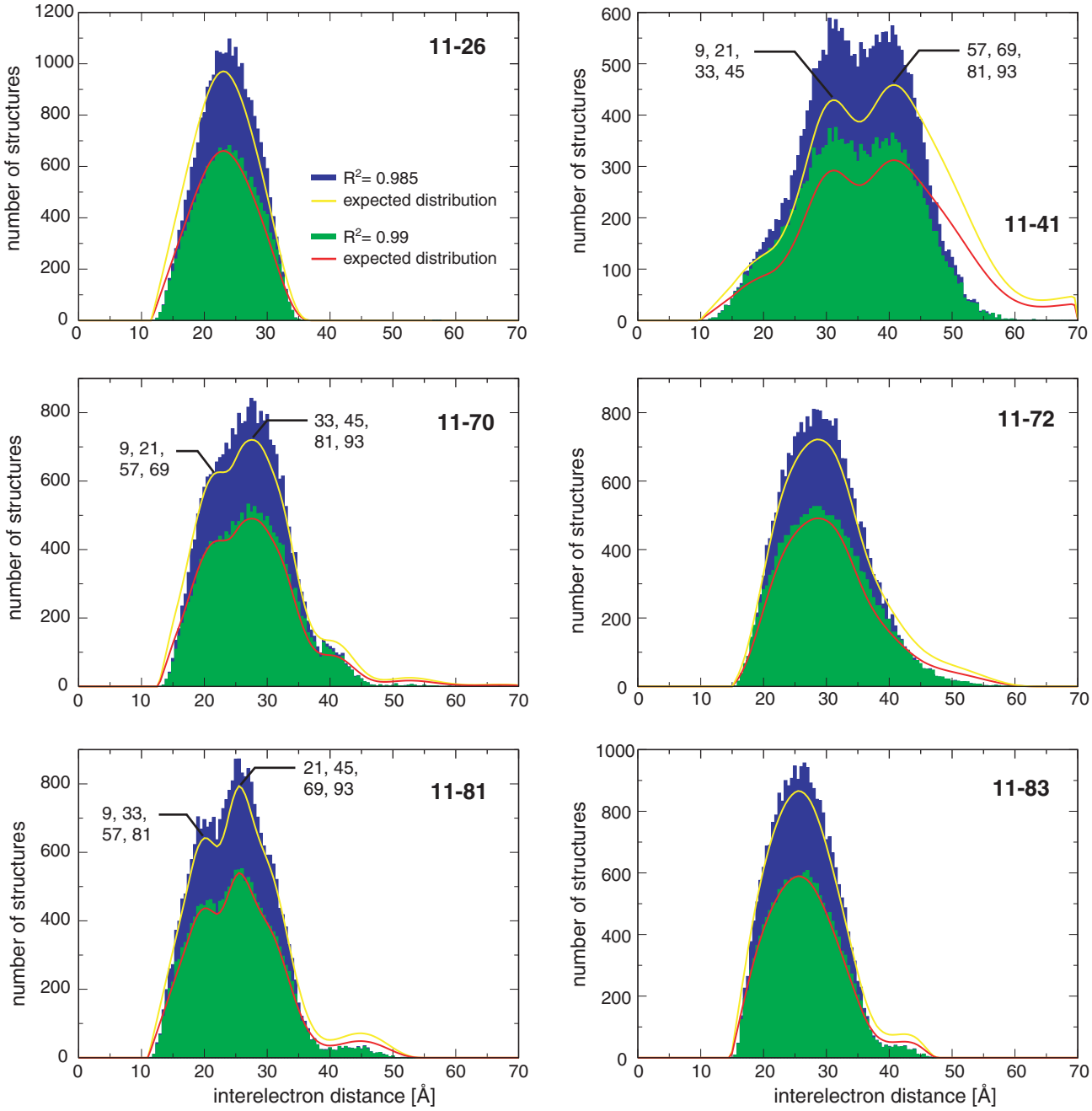

Supplementary Figure 6. Comparison of experimental and calculated ensemble distance distributions. Selected subpopulations associated with the distribution maxima are indicated (c.f. Supplementary Table 2).

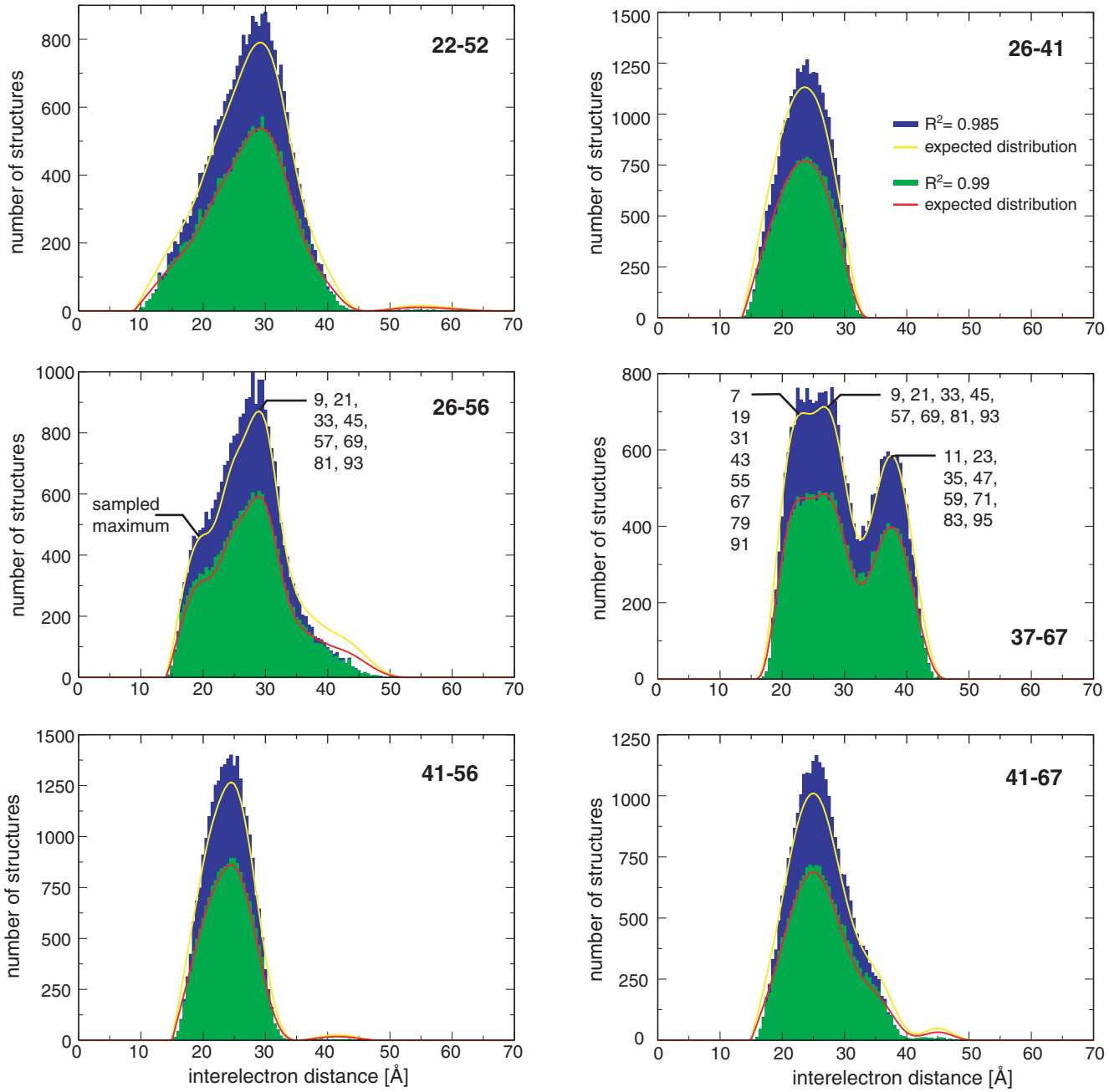

Supplementary Figure 6, continued.

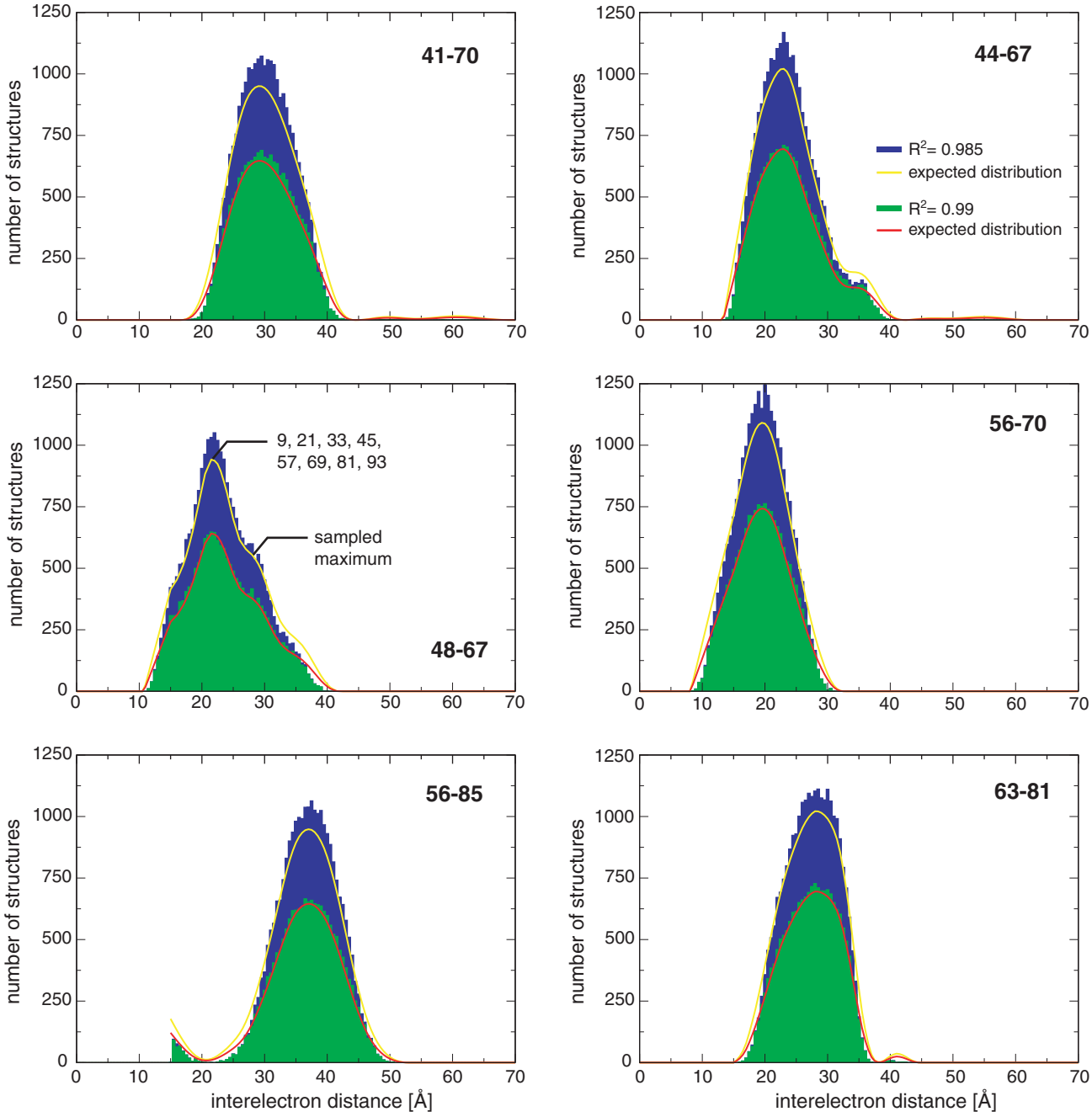

Supplementary Figure 6, continued.

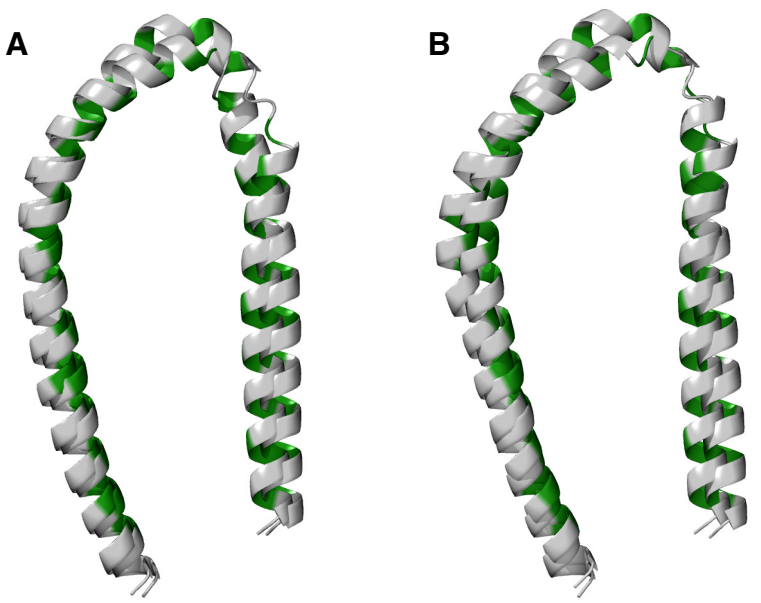

Supplementary Figure 7. Comparison of subpopulation 93 C′N′/same average representatives. (**A**) Representatives obtained for two independent repeat ensemble calculations (5,000 structures each) with permissive $\chi_{1\text{-}3}$ intervals of ±30° around their nominal values (see Experimental Procedures). Between the average representatives, an r.m.s.d. of 2.0 Å was obtained for helix-N′ (Asp2-Lys32) and helix-C′ (Ser42-Thr92) backbone coordinates. (**B**) Representatives from ensembles calculations (5,000 structures each) with $\chi_{1\text{-}3}$ intervals of ±30° and ±10°, respectively. As a consequence of this tightening, the number of structures encountering any violation of structural constraints increased slightly from 3.0% to 5.0%, but for C′N′/same structures the r.m.s. differences to the mean coordinates remained virtually constant at 4.7 Å. Between the average representatives, an r.m.s.d. of 2.3 Å was obtained for helix-N′ and helix-C′ backbone coordinates. The hydrophobic helix faces are colored in *green*.

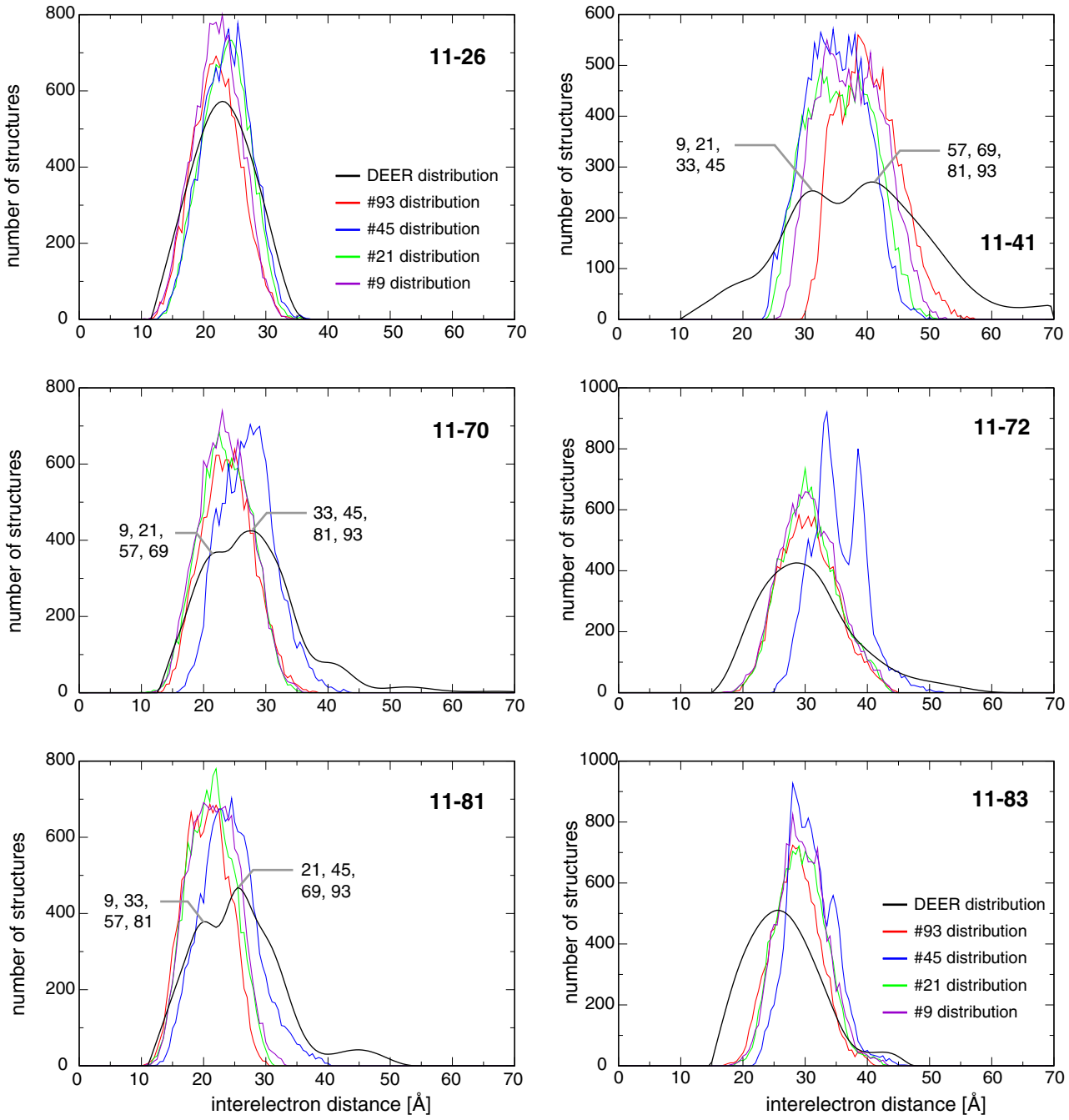

Supplementary Figure 8. Reconstruction of distance distributions from C′N′ subpopulation structures. For subpopulations 9, 21, 45 and 93, 86.7, 82.1, 86.4% and 75.6% of simulated annealing calculations resulted in canonical spin label orientations (15,483, 14,669, 15,435 and 13,510 structures). The expected DEER distribution for 15,483 structures is depicted. If a target interelectron distance maximum is underrepresented in the reconstruction effort of a specific interelectron distance distribution, the underlying backbone structure must have preferentially pointed at least one spin label in a suboptimal direction, which is indicative of an invalid subpopulation. Such a "computational bias" may have arisen during average representative calculations if a relatively flexible spin label did not pull its associated backbone segment in a correct orientation, but rather was driven away from its default orientation. The opposite situation, an "environmental bias" of a spin label that is computationally not reproduced, is also possible, but, for the present system, was expected to be small. 11R1-72R1 and 11R1-83R1 exhibit offsets of 1.6 and 3.0 Å, respectively, to Gaussian distribution fits to subpopulation 93 (30.1±4.7 Å and 28.5±3.9 Å, respectively). For 11R1-70R1 and 11R1-81R1 the offset to the correct maxima is 3.8 and 5.0 Å, respectively, for subpopulation 93 (Gaussian fits of 23.7±4.3 Å and 20.5±3.8 Å).

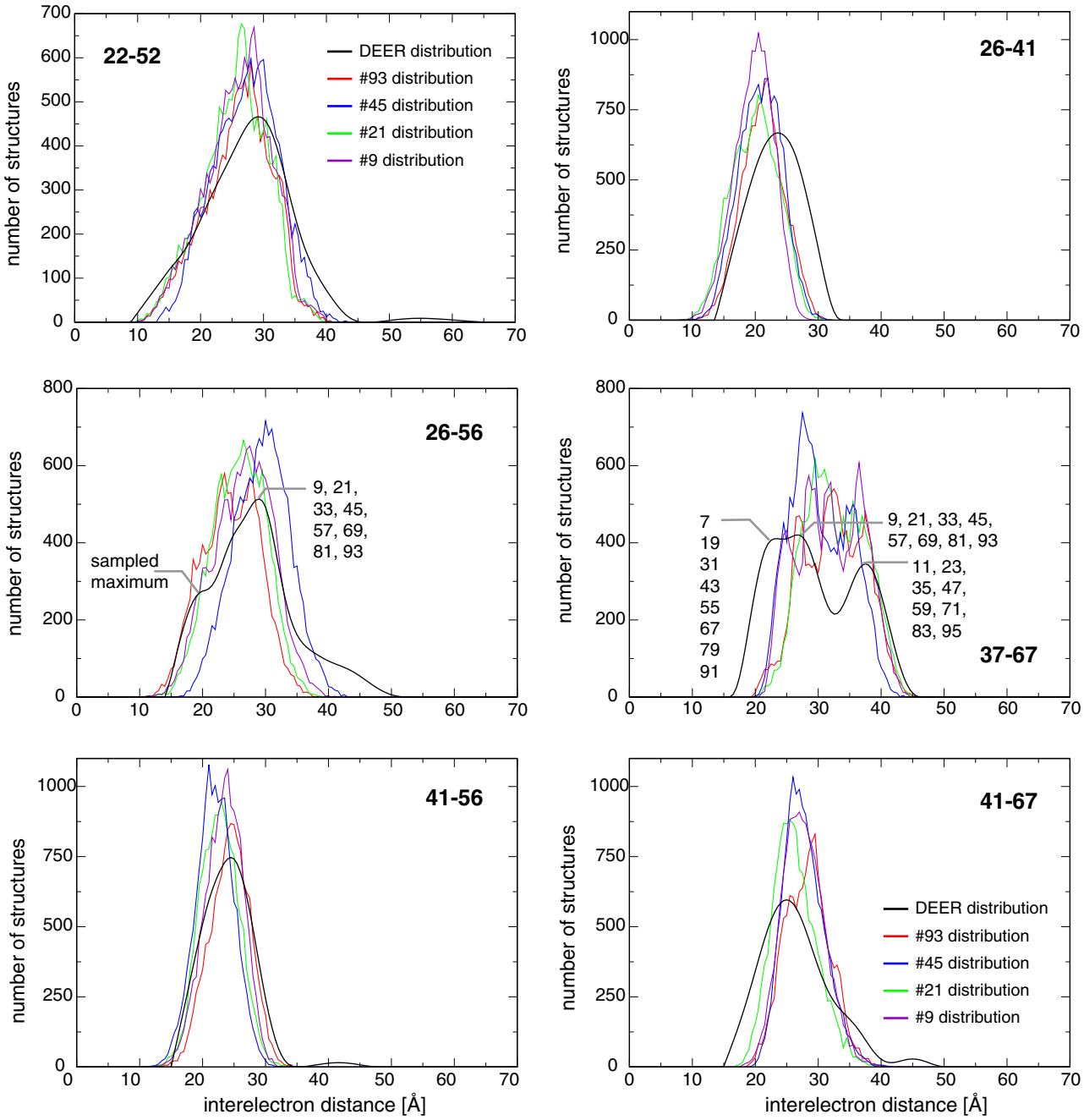

Supplementary Figure 8, continued. With the exception of 37R1-67R1, the depicted interelectron distributions were well reproduced. The center maximum of 37R1-67R1 was reproduced, but the distribution is not well centered. 37R1 is located at the center of the helix-helix linker and its conformation is dynamically disordered, making a reconstruction of its distribution difficult and less meaningful. 22R1-52R1 is the only non-linked distance pair (see main text). 26R1-41R1 exhibits an offset of 2.3 Å to a Gaussian distribution fit to subpopulation 93 (21.2 ± 3.4 Å). In general, 26R1-41R1 would prefer to be at greater distances than reconstructed, but this desire is apparently spoiled by the sum of all other structural restraints. Assuming all other structural restraints are correct, this would indicate a slight environmental or computational bias of 26R1 along the 26R1-41R1 interelectron vector (Fig. 1B). Such deviations between experimental and reconstructed maxima also represent an explanation for having experienced worse structural convergence when sampling distance maxima with ±1.5 Å rather than ±2.5 Å in the calculation of average representatives.

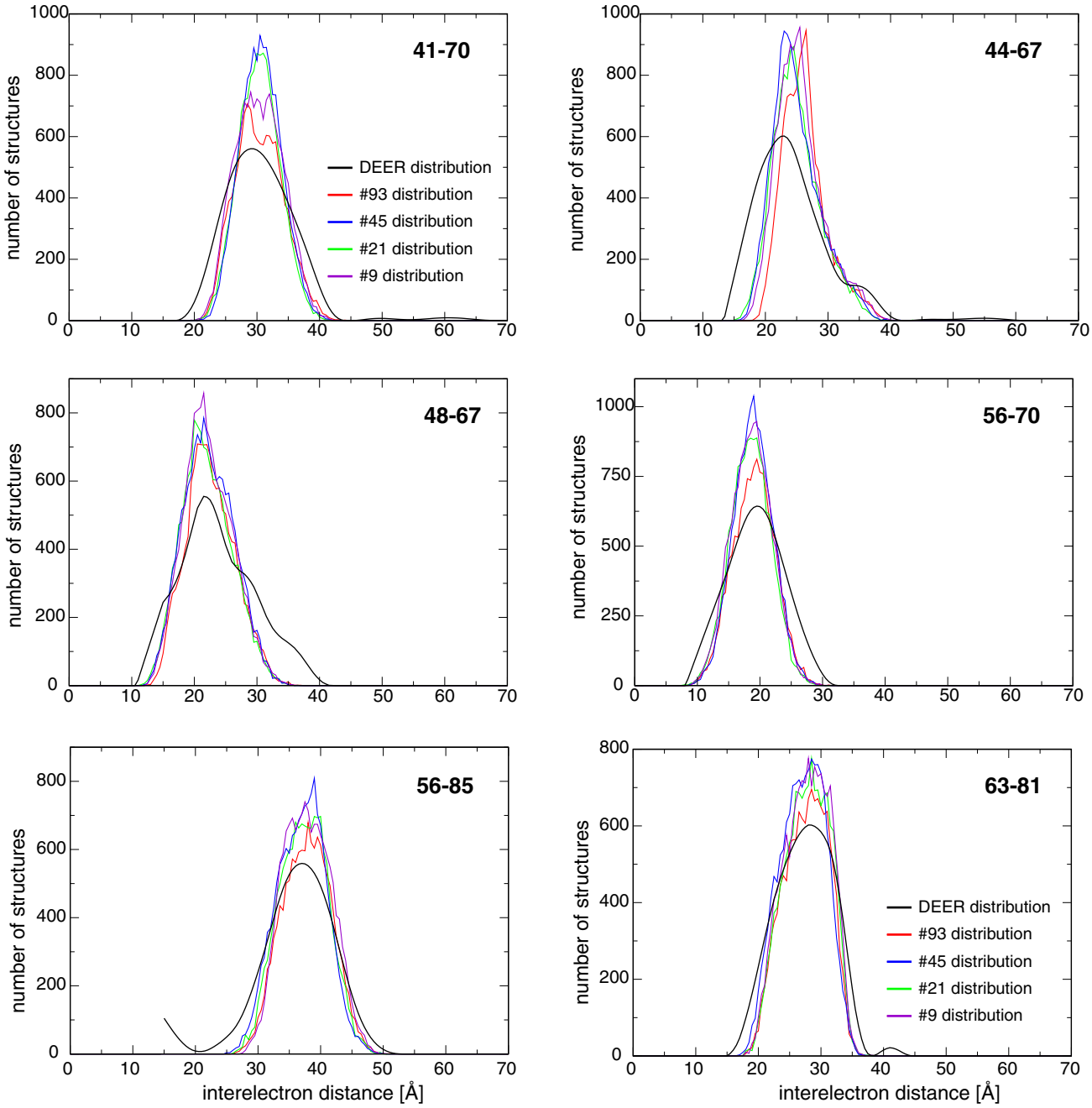

Supplementary Figure 8, continued. The six depicted interelectron distributions were well reproduced. 44R1-67R1 exhibits a small offset of 1.5 Å to a Gaussian distribution fit to subpopulation 93 (25.5 ± 3.1 Å).

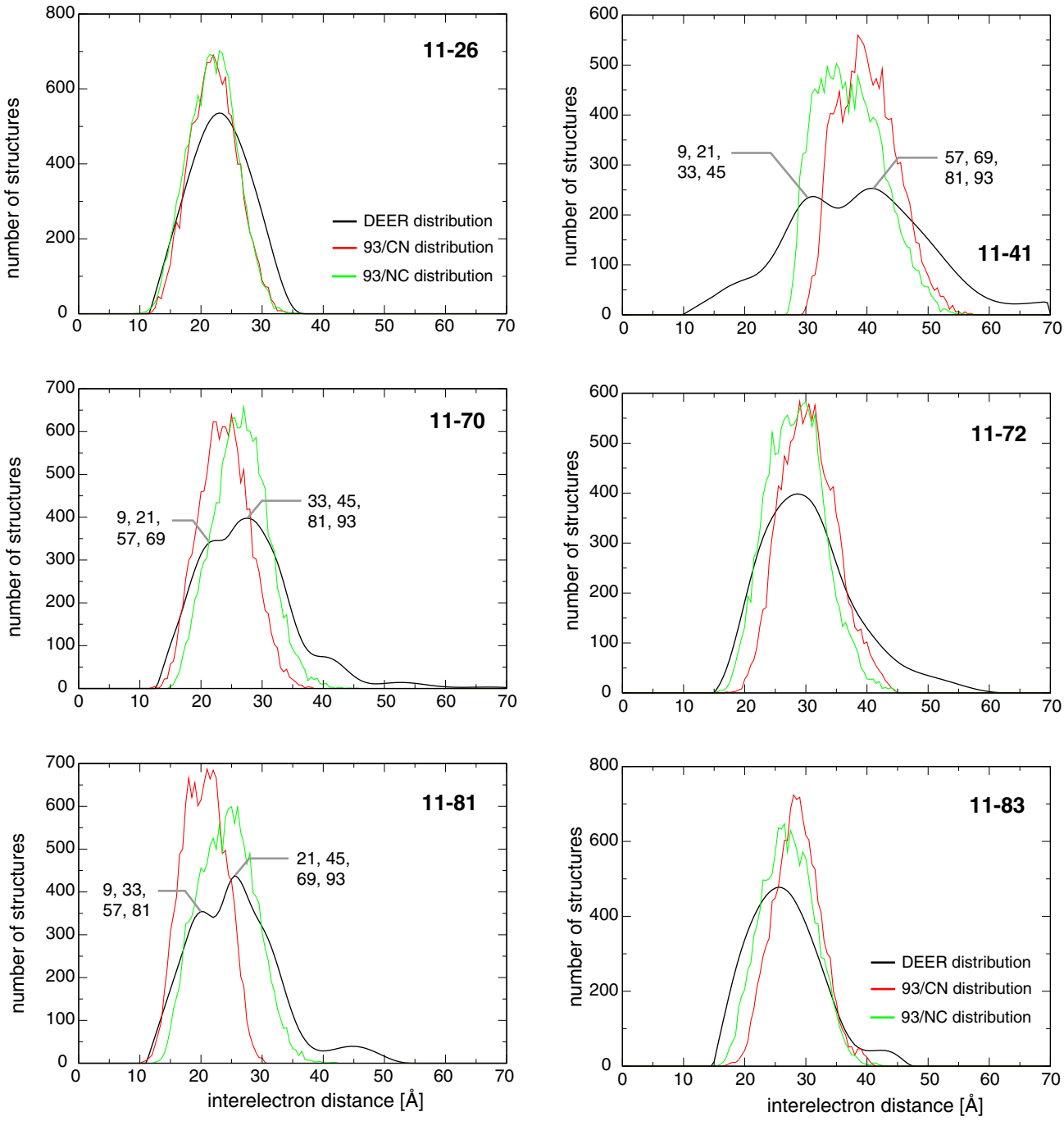

Supplementary Figure 9. Reconstruction of distance distributions from 93/N′C′/same and 93/C′N′/same subpopulation structure. For the C′N′ and N′C′ orientations 75.6% and 81.1% of simulated annealing calculations resulted in canonical spin label orientations (13,510 and 14,488 structures). The expected DEER distribution for 14,488 structures is depicted. 93/N′C′/same populated the correct target interelectron distance maxima.

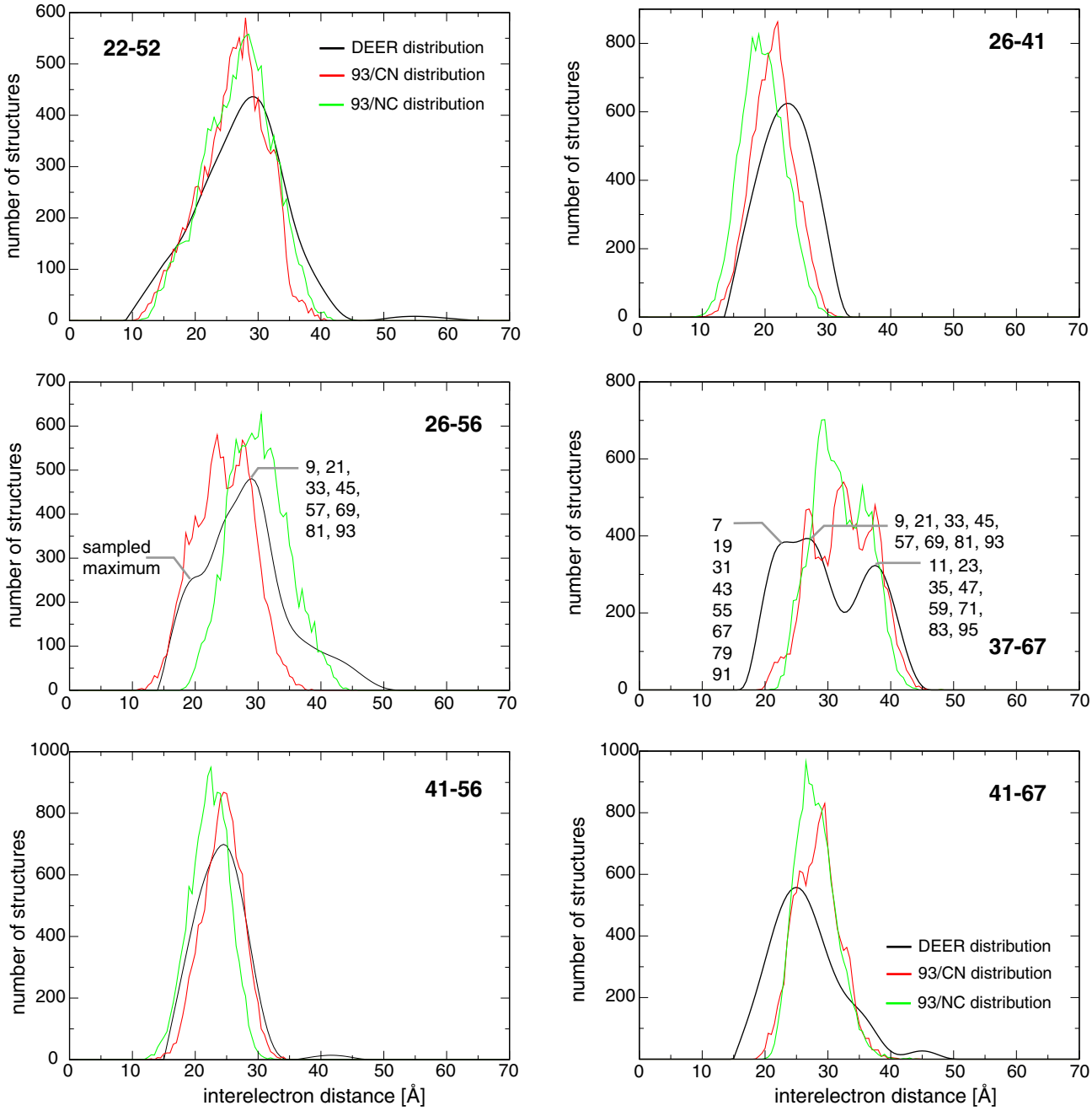

Supplementary Figure 9, continued. With the exception of 37R1-67R1, the depicted interelectron distributions were well reproduced for 93/N′C′/same. The center maximum of 37R1-67R1 was reproduced, but the distribution is not well centered. 37R1 is located at the center of the helix-helix linker and its conformation is dynamically disordered, making a reconstruction of its distribution difficult and less meaningful.

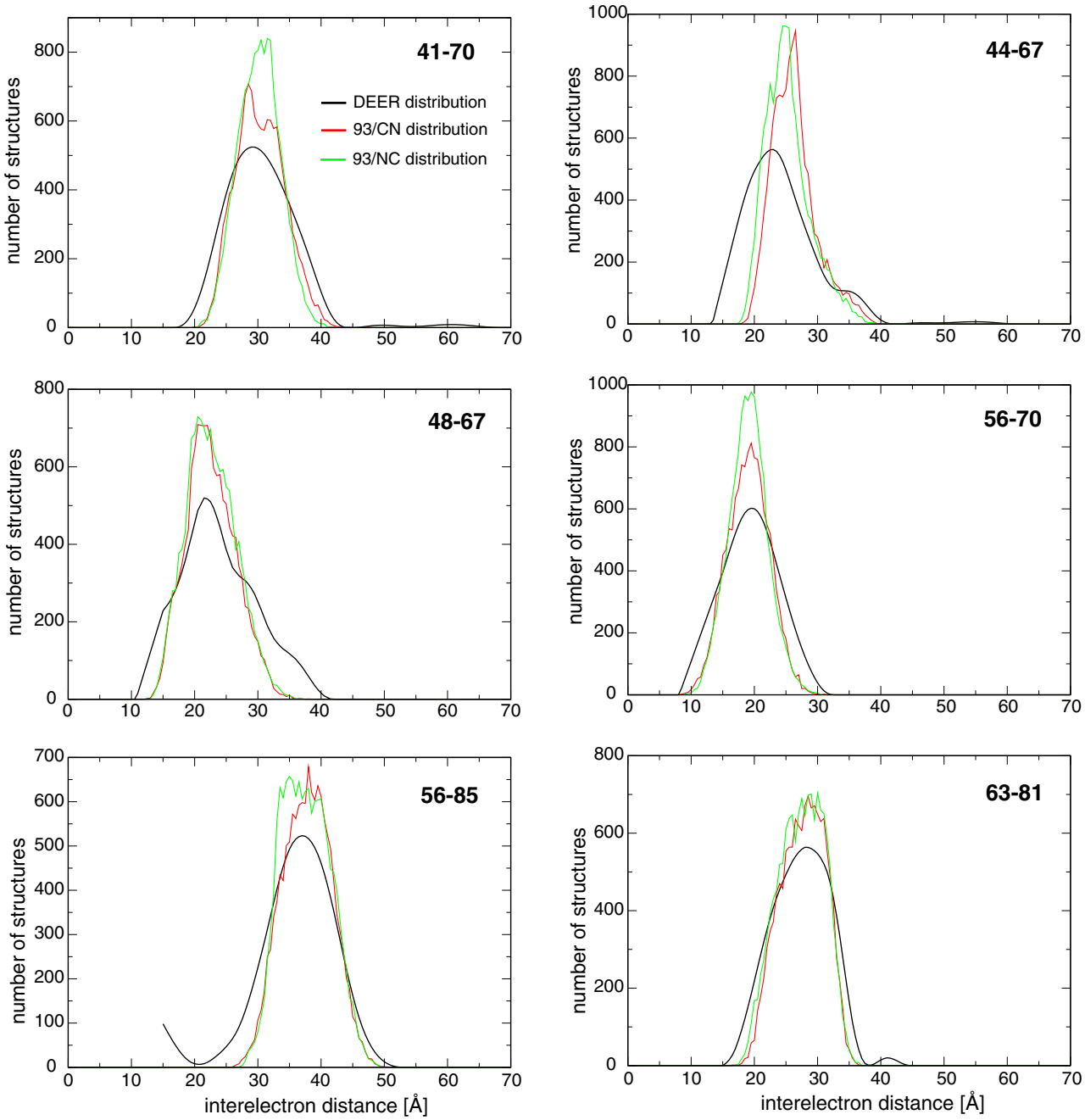

Supplementary Figure 9, continued.

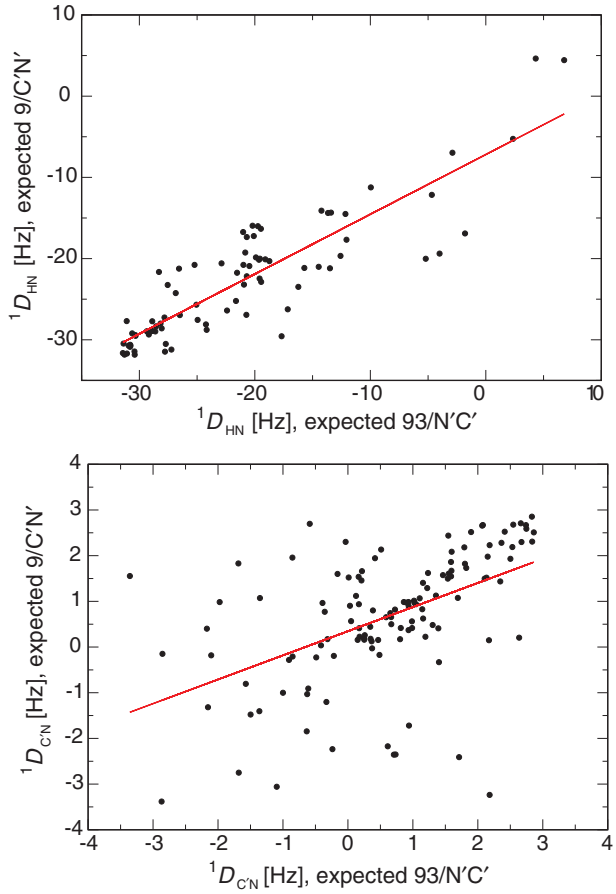

Supplementary Figure 10. Expected residual dipolar couplings (RDC) for 9/C′N′/same and 93/N′C′/same structures. Expected $^1D_{NH}$ and $^1D_{NC}$ couplings for residues 3-92 of the 9/C′N′/same and 93/N′C′/same structures were computed by back-calculating RDC employing tensor parameter obtained by fitting the segments of highest experimental Da values (residues 10-18 and 74-81) to each individual structure. Correlation coefficient, R, of 0.876 and 0.504 were obtained for $^1D_{NH}$ and $^1D_{NC}$ couplings, respectively.

References

(1) Milov, A. D.; Naumov, B. D.; Tsvetkov, Y. D. *Appl. Magn. Reson.* **2004**, *26*, 587-599.

(2) Wishart, D. S.; Case, D. A. In *Nuclear Magnetic Resonance Of Biological Macromolecules, Pt A* 2001; Vol. 338, p 3-34.

(3) Spera, S.; Bax, A. *J. Am. Chem. Soc.* **1991**, *113*, 5490-5492.

(4) Lipari, G.; Szabo, A. *J. Am. Chem. Soc.* **1982**, *104*, 4546-4559.